Measurements of anomalous particle and energy fluxes in a magnetized plasma

S. V. Ratynskaia, V. I. Demidov, and K. Rypdal
Department of Physics, University of Tromsø, 9037 Tromsø, Norway
(Received 12 September 2001; revised manuscript received 27 February 2002; published 12 June 2002)

Electrostatic probe measurements of low frequency plasma fluctuations and anomalous particle and energy flux densities in a magnetized plasma are presented. A method allowing the simultaneous recording of instantaneous electric field, electron density, and temperature is invoked. The method is applied to flux density measurements in a weakly ionized, low beta plasma created in a toroidal device without magnetic rotational transform. It is also used to identify modes belonging to different dispersion branches and to obtain the dispersion relations for these modes. For the plasma states studied, the phase velocities and the cross phase between the electron density and electric field agree with those predicted from a local, linear stability analysis for electrostatic flute modes and drift waves. The instability threshold, however, is one order of magnitude higher than predicted by theory for unsheared flow. The fluxes measured are consistent with the estimated ionization rate.

DOI: 10.1103/PhysRevE.65.066403 PACS number(s): 52.25.Xz, 52.35.−g, 52.70.Ds

I. INTRODUCTION

Anomalous transport perpendicular to the magnetic field associated with electrostatic plasma turbulence has attracted considerable attention for the last few decades, particularly in connection with edge transport in fusion plasmas. In parallel to the mainstream fusion program, a number of linear and toroidal magnetized plasma devices without magnetic confinement have been constructed with the purpose of studying low frequency electrostatic turbulence and cross-field transport. The main idea is that the lower electron density and temperature in these devices, and the steady-state operating conditions facilitate the application of clusters of tiny plasma probes as diagnostics. A challenging diagnostic problem in this context is to perform accurate local measurements of instantaneous particle and energy density flux. The basic problem is the following: Suppose the z axis of a Cartesian coordinate system is directed along the ambient magnetic field and we want to measure the anomalous flux in the the x direction. Then simultaneous measurements of instantaneous values of electron density n, electric field E_y, and electron temperature T_e are necessary to obtain the anomalous cross-field flux densities [1]. Separating fluctuating quantities such as $n=\overline{n}+\tilde{n}$ into a time-averaged ($\overline{n}$) and a fluctuating ($\tilde{n}$) part, the time-averaged particle flux density can be written as $\langle\Gamma_x\rangle=\langle\tilde{n}\tilde{E}_y\rangle/B=\Sigma_{f>0}\Gamma_x(f)$, where

$$\Gamma_x(f)=\frac{2}{B}\sqrt{\langle|n(f)|^2\rangle\langle|E_y(f)|^2\rangle}\,\gamma_{nE}(f)\cos\alpha_{nE}(f). \quad (1)$$

Here f is frequency, B is magnetic field, $\gamma_{nE}(f)=|\langle n(f)E_y(f)^*\rangle|/\sqrt{\langle|n(f)|^2\rangle\langle|E_y(f)|^2\rangle}$ is the cross coherence, and $\alpha_{nE}(f)\equiv\arg\langle n(f)E_y(f)^*\rangle$ is the cross phase between n and E_y.

The average $\langle\cdot\rangle$ of the spectral quantities should be considered as an ensemble average over a large number of time records. The energy flux density can be written as $\langle Q_x\rangle=\frac{3}{2}\langle\tilde{E}_y\tilde{p}\rangle/B=\frac{3}{2}T_e\Gamma_x+\frac{3}{2}n\langle\tilde{E}_y\tilde{T}_e\rangle/B=\Sigma_{f>0}Q_x(f)$, where

$$Q_x(f)=\frac{3}{2}T_e\Gamma_x(f)+\frac{3}{B}|\langle T_e(f)E_y^*(f)\rangle|\cos\alpha_{TE}(f). \quad (2)$$

If the dominant modes have cross phases $\alpha(f)$ close to $\pi/2$ or $3\pi/2$ [i.e., $|\cos\alpha(f)|\ll 1$], the respective fluxes become very sensitive to errors in the measurements of $\alpha(f)$. Such errors will arise, for instance, if one does not succeed in eliminating the influence of $\tilde{T}_e$ on the measurements of $\tilde{V}_{pl}$ and $\tilde{n}$. In this paper we propose a method to deal with this problem in the context of Langmuir probe measurements. Probe measurements of the fluxes in magnetic confinement devices have been reported in a number of papers [2–5], and some attempts have also been made to correct for the temperature fluctuations [6,7]. However, the problems of applying Langmuir probes under those plasma conditions are very different from the cold, low density, and often partially ionized plasmas one deals with in nonconfinement devices. Measurements of E_y by recording the floating potential on two probe tips separated poloidally were carried out in a Q machine by Nielsen *et al.* [8]. The density fluctuations were derived from the ion saturation current, and hence the particle flux spectrum could be estimated. The very low $\tilde{T}_e$ in Q machines could serve as a justification for this method, but it certainly can yield errors in some other devices where temperature fluctuations are important. It should also be emphasized that the application of a valid probe theory becomes a particularly important issue for measurements in a magnetized plasma, since theories for unmagnetized plasma might give rise to significant errors in the interpretation of probe data.

II. INSTANTANEOUS MEASUREMENT OF FLUID OBSERVABLES

The proposed probe system for measurements of anomalous particle and energy fluxes consists of two conventional cylindrical probes and two cylindrical probes equipped with insulating end plugs. The cluster is simple in operation and does not require voltage sweeps. It allows us to separate and

measure simultaneously the fluctuating quantities $\tilde{n}$, $\tilde{V}_{pl}$, $\tilde{E}$, and $\tilde{T}_e$.

A. Measurements of $\tilde{V}_{pl}$ and $\tilde{E}$

The plug probe [9] is a modified cylindrical Langmuir probe oriented parallel to the magnetic field, which floats at a potential V_f close to the plasma potential V_{pl}. This shift of V_f towards V_{pl} is due to a strong reduction of the electron to ion saturation current ratio I_e^{sat}/I_i^{sat} caused by the insulating end plugs. The simple geometry of the plug probe suggests that the probe characteristic can be obtained by means of a modified theory for a conventional cylindrical probe in a magnetized plasma [10]. The modification is simply a reduction of the electron current by a numerical factor determined experimentally. This model has been shown to give a good agreement between the experimental and theoretical curves with the floating potential very close to the plasma potential. It allows us to demonstrate that the fluctuations in V_f due to T_e fluctuations are reduced by almost an order of magnitude compared to the conventional probe. The same can be found from the experimental ratio of amplitude spectra of the floating potential measured by a conventional probe and a plug probe. A comparison between measurements of time-averaged plasma potential by plug probes and emissive probes demonstrates agreement between the two methods within an accuracy of T_e/e. Analysis of the first derivative of a conventional probe characteristic in magnetized plasma [11] yields V_{pl}, which also agrees with V_f of the plug probe within an accuracy of T_e/e. A better agreement cannot be expected since both emissive probes and first derivative methods have uncertainties of order T_e/e due to the space charge effect [12] and plasma potential fluctuations [11], respectively. Plug probe measurements of plasma potential have been performed with a wide range of probe lengths, probe radii, and plug sizes. When these are within certain limits they all give consistent results, indicating that the influence of the the electron temperature is effectively eliminated by the plugs and the parallel probe orientation.

The evidence presented above shows that the plug probe correctly applied under the plasma conditions studied in this paper provides an accurate instantaneous measurement of the plasma potential, and, in particular, it reduces drastically the influence of electron temperature fluctuations on the measurement. Thus, by subtracting the signals from two spatially separated plug probes, one obtains a direct measurement of the instantaneous perpendicular electric field component in the direction of the separation vector between the probes. The traditional way of making this E-field measurement, originally introduced by Powers [13], is to measure the plasma potential fluctuations in one location and use the relation $E(f) = -ik(f)V_{pl}(f)$. This requires that the plasma potential can be represented as a superposition of modes with one well defined dispersion branch, and that we have an independent measurement of the dispersion relation $k(f)$ for this branch. In Sec. IV B it is demonstrated that in some of our measurements there are two dispersion branches, the plasma potential fluctuations are dominated by one mode branch while the electron temperature fluctuation by the other. However, the floating potential of a conventional probe, which is often used for the measurement of $k(f)$, is given as a linear combination of plasma potential and electron temperature, and an attempt to determine $k(f)$ for the former mode branch from this signal will give incorrect results. The direct measurement of the electric field suggested above is not based on any assumption about the wave nature of the fluctuations and is, therefore, the prefereable approach.

B. Measurements of $\tilde{n}$

The fluctuations of the density can be found from the electron or ion saturation current. For magnetized plasmas and the hydrodynamic regime of probe operation, the saturation currents are functions of not only $\tilde{n}$ but also $\tilde{T}_e$ [10]. The influence of the latter can be eliminated if simultaneous measurements of $\tilde{T}_e$ are provided.

C. Measurements of $\tilde{T}_e$

For such measurements we suggest to utilize the floating potential of a conventional probe [9] in conjunction with the plasma potential measured by a plug probe. The floating potential V_f is the probe potential at which the ion current is equal to the electron current, and is given by $V_f = V_{pl} - \mu T_e/e + V_0$, where T_e is in energy units and e is the proton charge. Conventionally, μ is calculated from theory for collisionless, unmagnetized plasma. In magnetized plasma, however, the current ratio, and therefore μ and V_0, strongly depend on the magnetic field strength and the probe size and orientation. The validity of this formula can be verified and μ and V_0 can be determined experimentally for particular plasma conditions (see Sec. III). Thus, the fluctuating part of T_e is given as

$$\tilde{T}_e = e\frac{\tilde{V}_{pl} - \tilde{V}_f}{\mu}. \tag{3}$$

Thus, the proposed combination of two plug probes and two conventional probes provides an instantaneous measurement of all quantities needed to obtain the instantaneous particle and energy flux density in a given direction. A detailed description of the probe cluster employed in this paper is given in the following section.

III. EXPERIMENTAL ARRANGEMENT

The method is tested and verified in the simple magnetized torus ''Blaamann'' [14]. The plasma is produced by electron emission from a hot negatively biased cathode filament suspended vertically near the center of the plasma column. This creates a negative potential well in the poloidal cross section of the plasma column with weakly elliptic equipotential curves elongated in the vertical direction. The potential well leads to a poloidal plasma rotation with a sheared $\mathbf{E}\times\mathbf{B}$ flow along the equipotential surfaces. The depth and shape of the potential well is determined by the perpendicular ion mobility due to ion-neutral collisions (or the Pedersen

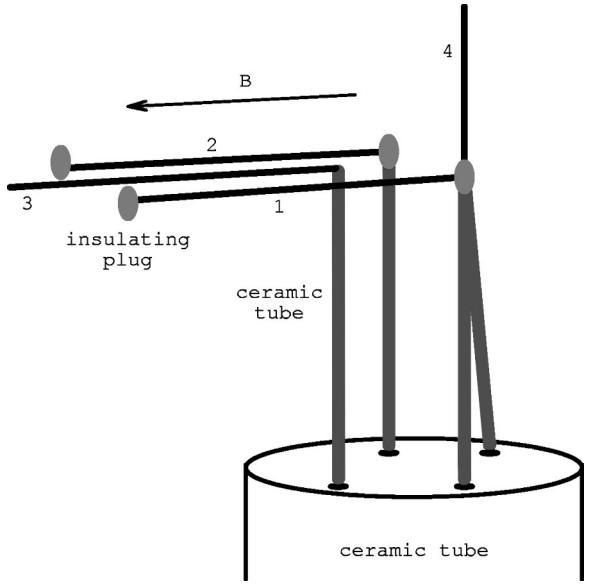

FIG. 1. A sketch of the probe cluster for flux measurements. (1), (2) are plug probes parallel to the magnetic field, (3) and (4) are conventional probes parallel and perpendicular to the magnetic field, respectively. Not to scale.

conductivity). The current driven by the radial electric field $\overline{E}_r = -\partial \overline{V}_{pl}/\partial r$ is

$$I_{dis} \approx -4\pi^2 R_0 \sigma_P r \frac{\partial \overline{V}_{pl}}{\partial r}, \tag{4}$$

where $\sigma_P = n m_i \nu_{in}/B^2$ is known as the Pedersen conductivity, m_i is the ion mass, ν_{in} is the ion-neutral collision frequency, $R_0 = 0.65$ m is the major radius of the torus, and r is the local minor radius coordinate. The discharge current I_{dis} flowing in the external circuit corresponds to the charge per unit time in the form of primary electrons injected into the flux tube intersecting the hot cathode. This charge is compensated by an inward radial current given by Eq. (4). If I_{dis}, ν_{in}, and $\overline{n}(r)$ are known, the potential profile $\overline{V}_{pl}(r)$ can be found from Eq. (4).

The experiments are conducted with the following discharge parameters: Helium neutral gas pressure $p = 0.3$ Pa, magnetic field $B = 0.15$ T, discharge current $I_{dis} = 1$ A, discharge voltage $V_{dis} = 140$ V. For these conditions the typical plasma density is $n \sim 3 \cdot 10^{17}$ m^3, electron temperature is $T_e \approx 1.5$ eV and the ion temperature $T_i \approx 0.2$ eV.

The probe system for flux measurements shown in Fig. 1 consists of two plug probes (1) and (2) parallel to each other and to the magnetic field and separated by 6 mm in the poloidal direction. The rods are molybdenum wires with radius $R = 0.125$ mm and length $L = 10$ mm. The plugs are made by several applications of a ceramic glue to the ends of the rods. A conventional molybdenum cylindrical probe (3) with $R = 0.125$ mm and $L = 10$ mm is parallel to the probes (1) and (2) and to the magnetic field. Another cylindrical molybdenum probe (4) with $R = 0.125$ mm and $L = 5$ mm is perpendicular to the probes (1)–(3) and to the magnetic field.

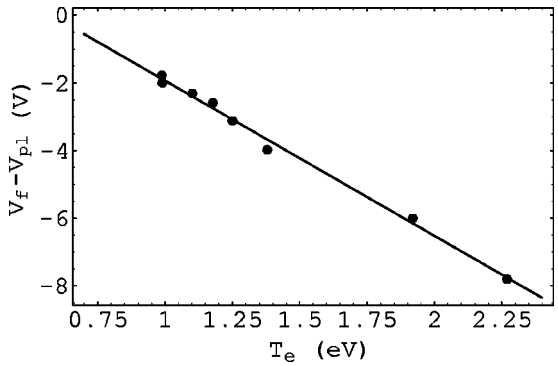

FIG. 2. Experimental determination of μ and V_0. The coefficients $\mu = 4.6 \pm 0.2$ and $V_0 = (2.6 \pm 0.2)$ V are obtained from fitting a linear function (full line) to the data (dots).

$\tilde{T}_e$ is determined from Eq. (3), where V_f is the floating potential measured by the perpendicular probe (4) and V_{pl} is the floating potential from the plug probe (1), which has the same poloidal position as probe (4). The radial extension of the perpendicular probe (4) could be a source of error if there were waves propagating radially. However, independent simultaneous measurements at different radial positions show that there is no detectable phase difference between the signals at two radial positions separated by 5 mm. One should be aware, though, that if the perpendicular probe is not directed perpendicular to the direction of the wave propagation, one could run into problems with this particular design of the probe cluster.

The value of μ is obtained experimentally by measurements of $\overline{V}_f - \overline{V}_{pl}$ as a function of $\overline{T}_e$ in various points of plasma the with different electron temperatures. The coefficients $\mu = 4.6 \pm 0.2$ and $V_0 = (2.6 \pm 0.2)$ V are obtained from fitting a linear function to the data as presented in Fig. 2.

Note that inaccuracies in μ affect only the amplitude of $\tilde{T}_e$ but not its spectral characteristics and phase. However, inaccuracies in μ and the magnitude of $\tilde{T}_e$ may influence significantly the density measurements and its phase, and thus the resulting flux. For measurements of $\tilde{n}$ the electron saturation current is convenient to use, since under the actual experimental conditions, the Bohm formula [10] for the electron saturation current to the parallel probe (3) takes the simple form $n = -I_e^{sat} B/8RT_e$, as shown in Ref. [15].

For the flux measurements, 10^6 data points of $\tilde{V}_f$ from each of the plug probes (1) and (2) and the perpendicular probe (4) and electron saturation current from the parallel probe (3) are sampled simultaneously at 100 kHz. The averaged electron temperature $\overline{T}_e$ is measured from the first derivative of the probe current with respect to the potential by fitting the curve obtained from a probe kinetic model [11] to the experimental curve for the derivative.

Another probe cluster is applied for measurements of dispersion relations for the unstable modes (see Sec. IV B). It consists of two identical probe pairs, each consisting of a parallel plug probe and a perpendicular probe in the same poloidal location. The probe pairs are separated poloidally by 6 mm. Each probe pair provides temperature fluctuations at

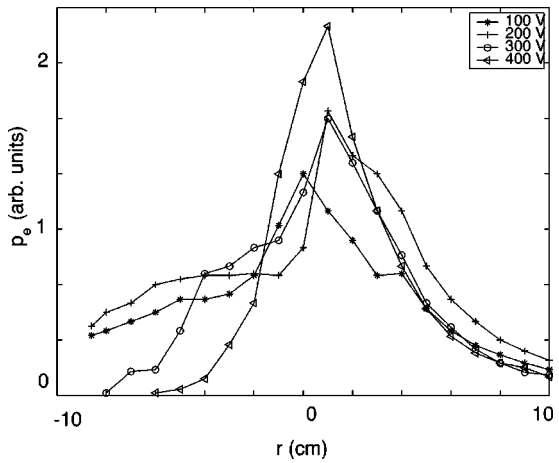

FIG. 3. Measured electron pressure profiles for different values of the discharge voltage, $V_{dis}=100$, 200, 300, 400 V. Ionization source is roughly proportional to V_{dis}.

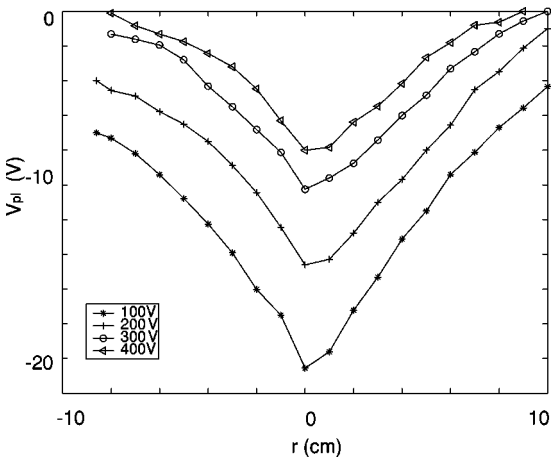

FIG. 4. Measured plasma potential profiles for different values of the discharge voltage, $V_{dis}=100$, 200, 300, 400 V.

the poloidal location of the pair and the two pairs allow us to measure the cross phase between the $\tilde{T}_e$ signals from their respective poloidal locations. The floating potential of the two plug probes provide cross phases for the $\tilde{V}_{pl}$ signals at the same two poloidal locations.

The alignment of the parallel probes (1)–(3) in Fig. 1 along the magnetic field is essential for correct operation. Optimal alignment is obtained by taking the characteristics of the probes and rotating them until minimal I_e^{sat} is achieved. For flux measurements is it useful to rotate the cluster by 180° and check that cross phases between corresponding quantities have changed by π and the flux has changed sign. The robustness of the method has been tested by application of clusters with different probe sizes and distances between the probes, and has been shown to yield consistent results.

IV. EXPERIMENTAL RESULTS AND INTERPRETATION

Fluctuations and radial anomalous transport in a particular discharge of the simple torus have been investigated by recording fluctuation data at a few points in the equatorial plane along the major radius. Positive *r* along the horizontal axes refers to the positions outside the center of the cross section, and negative values to those inside of the center. On the outer slope the pressure gradient is directed opposite to the magnetic field radius of curvature, which favors the electrostatic interchange instability for flute modes ($k_\parallel=\mathbf{k}\cdot\mathbf{B}/B=0$). This instability is driven by the electron pressure gradient, and has positive growth rate only if the ratio between the radius of curvature of the magnetic field lines *R* and the pressure scale length *L* exceeds a critical value [16,17]. Figure 3 shows experimental pressure profiles that on the outside slope are exponential $p_e \propto \exp(-r/L)$, and where *L* remains almost independent of the strength of the plasma source (and hence the radial plasma flux). The pressure gradient is almost ten times steeper than that corresponding to the linear instability threshold in a plasma without shear flow, which is discussed in Sec. IV A [Eq. (5)], but agrees well with the gradient scale length observed in the global simulations of the simple torus plasma. The robustness of the outside profile and its scale length is an indication that the profile remains close to a linear stability threshold and hence that the most unstable mode is marginally stable.

Figure 4 shows the corresponding potential profiles, demonstrating that the radial electric field is approximately inversely proportional to the plasma density, as it should be since the Pedersen conductivity is proportional to this density.

A. Local stability analysis

A local stability analysis of flute modes and drift waves in a slab with a magnetic field of radius of curvature R_0 and exponential density profile $n\sim\exp(-r/L)$ has been performed by Garcia [17]. The analysis was made for isothermal electrons, but can easily be generalized to include electron temperature fluctuations. For a plasma without flow, flute modes ($k_\parallel=0$) are unstable only on the outside density slope, where the density gradient points in the opposite direction of the radius of curvature of the magnetic field. The instability condition for a mode with vertical wave number k_y and $k_R=0$ is $\epsilon\equiv R_0/2L>1+\rho_s^2k_y^2/4$, where *L* is the density gradient scale length and $\rho_s=c_s/\omega_{ci}$ is the Larmor radius of an ion with electron temperature. Smaller k_y are more unstable than larger, but since the smallest possible wave number in a slab with vertical extent L_y is $k_y=2\pi/L_y$, the instability condition becomes $L<L_{thr}$, where

$$L_{thr}=\frac{R_0}{2(1+\pi^2\rho_s^2/L_y^2)}\approx\frac{R_0}{2}. \tag{5}$$

At the threshold $L=L_{thr}$ the smallest possible wave number $k_y=2\pi/L_y$ is marginally stable and all higher wave numbers are linearly stable. Stable and marginally stable flute modes have a cross phase between electron density and plasma potential equal to $\alpha_{nV}(k)\approx\pi$. The threshold for the flute inter-

change instability is due to the stabilizing effect of the compression term $n\nabla\cdot\mathbf{v}_E=-(2n/RB)\partial_y V_{pl}$ in the continuity equation. This term, and the corresponding threshold, is due to magnetic field curvature and does not occur in the gravitational interchange instability.

While flute modes are driven unstable by field curvature on the weak field side (i.e., on the outside slope) of the torus cross section, drift waves do not require field curvature for instability, and can be unstable both on the outside and inside slopes. However, on the outside slope the compression term creates the same threshold as for flute modes. For long wavelength drift modes ($k_\perp\rho_s\ll 1$) the growth rate and cross phase $\alpha_{nV}(k)$ depend on the parameter

$$\psi=\frac{\omega_{ci}}{\nu_e}\frac{k_\parallel^2 L}{k_y^3\rho_s^2}. \tag{6}$$

In the hydrodynamic limit $\psi\ll 1$, one finds that $\alpha_{nV}(k)\rightarrow\pi/4$, $n(k)/n_0\gg eV_{pl}(k)/T_e$, and the growth rate $\gamma(k)\propto k_\parallel^2/\nu_e$. In the adiabatic limit $\psi\gg 1$ we have $\alpha_{nV}(k)\rightarrow 0$, $n(k)/n_0\approx eV_{pl}(k)/T_e$, and $\gamma(k)\propto\nu_e/k_\parallel^2$. The results quoted here are valid for a situation without a shear flow. Studies of the gravitational instability indicate that velocity shear should increase the stability threshold [18], but reliable results do not yet exist for the curvature driven instability.

Simple torus global modes with the structure $A(r)\exp i(m\theta+n\varphi-\omega t)$, where θ is the poloidal angle and φ the toroidal angle, will have parallel wave number $k_\parallel=n/R_0$ and perpendicular local wave number $k_\perp=m/r$. Here n and m are integers. By replacing k_y with $k_\perp$ in Eq. (6) we find for our experimental conditions that $\psi\approx 5n^2/m^3$. Flute modes correspond to $n=0$ and the dominant polodial mode number is $m=1$ (this is the mode that gives rise to the peak at $f=4.5$ kHz in the power spectra as discussed in Sec. IV B). For drift waves $n\geqslant 1$ and for the longest poloidal wavelengths ($m=1$), we have $\psi>5$, which corresponds to the adiabatic regime. For smaller wavelengths there is a transistion to the hydrodynamic regime.

B. Measurement of autopower and cross-power spectra

The power spectra of E, V_{pl}, n, and T_e measured at $r=+6$ cm are presented in Fig. 5. All spectra exibit a peak at 4.5 kHz. From earlier experiments [16,19,20] it is known that this peak is due to flutelike, large-scale, coherent structures that move with the poloidal plasma rotation. At lower neutral gas pressures these structures live for several rotation periods, but for the pressure applied in these experiments the structures apparently grow due to the interchange instability on the outside passage, but are considerably dissipated on the inside, since the spectral peak is almost absent at $r=-6$ cm (spectra at this position are not shown here). From Fig. 5 it is seen that about half of the total power in the density spectrum resides at frequencies above 6 kHz, where the spectrum has a power law dependence on frequency, $\langle|n(f)|^2\rangle\propto f^{-\eta}$. For density fluctuations the spectral index η is roughly 2, and for temperature and potential they are around 3 and 4, respectively. This means that the density

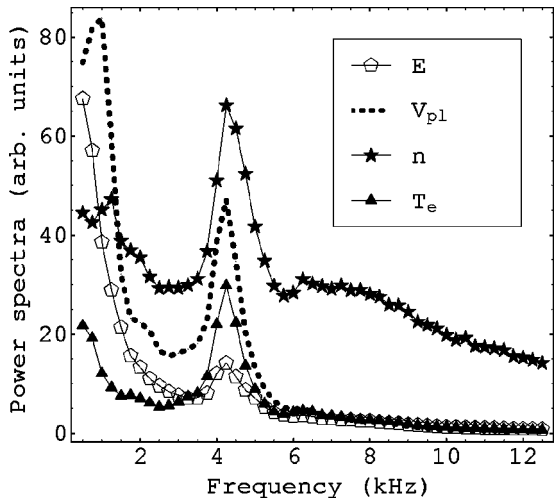

FIG. 5. Power spectra of electric field, plasma potential, density, and electron temperature at position $r=+6$ cm. Arbitrary units for each curve.

fluctuations dominate in the high frequency end of the spectrum. On the outside we find that $e\tilde{V}_{pl}/\overline{T_e}\approx -2\tilde{n}/\overline{n}$ and $\tilde{T}_e/\overline{T_e}\approx\frac{2}{3}\tilde{n}/\overline{n}$ for frequencies below 6 kHz. This is consistent with the adiabatic equation of state and the linear theory of flute modes [16]. On the inside ($r=-6$ cm) the spectral indices in the high frequency range are roughly the same as outside, and the fluctuation levels $\tilde{V}_{pl}$ and $\tilde{n}$ are of the same order of magnitude as outside. However, $\tilde{T}_e$ is reduced by a factor 3 compared to the outside for all frequencies. This indicates that parallel heat conduction plays an important role in the mode dynamics on the inside, which would be the case if drift waves ($k_\parallel\neq 0$) are dominant here.

At $r=+6$ cm the measured cross-phase spectra presented in Fig. 6 take the values $\alpha_{nE}\approx\alpha_{TE}\approx\pi/2$ and $\alpha_{nT}\approx 0$, consistent with flute mode dynamics and adiabatic equation of state. At $r=-6$ cm the mode phase velocities switch sign with respect to the probe pair measuring the poloidal electric field, so if the same modes propagate on the inside slope as on the outside slope, the cross phases α_{nE} and α_{TE} should be shifted by π, while α_{nT} should remain the same. What is actually observed, however, is that $\alpha_{nE}\approx\pi/2$ remains almost the same, $\alpha_{TE}\approx\pi$ is shifted by $\pi/2$, and $\alpha_{nT}\approx 3\pi/2$ is shifted by $3\pi/2$ compared to the outside position. On the outside slope $\alpha_{nE}\approx\pi/2$ corresponds to $\alpha_{nV}\approx\pi$, which is typical for flute modes. On the inside $\alpha_{nE}\approx\pi/2$ corresponds to $\alpha_{nV}\approx 0$ (since the wave number k_y has changed sign). This is characteristic for drift waves in the adiabatic regime, and indicates that density and electric field fluctuations are dominated by drift waves in this region. The relatively weak $\tilde{T}_e$ on the inside has a power spectrum peak at 4.5 kHz, suggesting that the temperature fluctuations here are associated with flute modes driven unstable on the outside and convected with the plasma flow (and damped) to the inside position. Since the density and potential fluctuations associated with these flute modes will be quite weak, we conclude that $\tilde{n}$ and $\tilde{V}_{pl}$ are dominated by the drift waves and $\tilde{T}_e$ by flute modes.

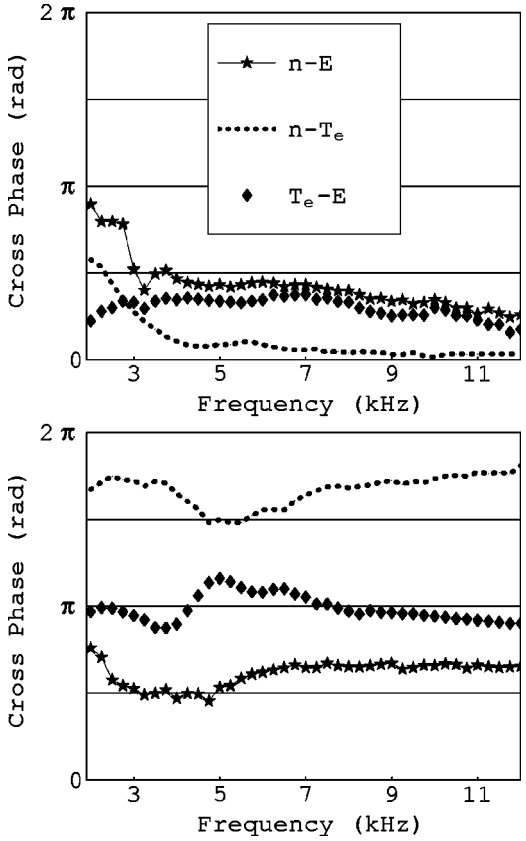

FIG. 6. Cross-phase spectra between density and electric field (α_{nE}), density and electron temperature (α_{nT}), and temperature and electric field (α_{TE}), measured at $r=+6$ cm (upper figure) and $r=-6$ cm (lower).

C. Measurement of dispersion relations

This picture is confirmed by comparing the cross phase between the plasma potential signal of two probes separated poloidally by a distance d to the corresponding cross phase between electron temperature signals (Fig. 7). In the position $r=-4$ cm the two cross-phases are different. The cross phase $\alpha_{12}(f)$ from the plasma potential measurement is determined by the potential fluctuations in drift waves, and yields the dispersion relation $k(f)=\alpha_{12}(f)/d$ for these waves in the laboratory frame. The cross phase from the temperature measurement is determined by temperature fluctuations in flute modes and depends on the dispersion characteristics of those modes. In the position $r=+4$ cm the two cross phases are the same, indicating that the fluctuations in $\tilde{V}_{pl}$ and $\tilde{T}_e$ are both dominated by flute modes in the outside position. The dispersion curves $k(f)$ are approximately straight lines and their inverse slopes give the phase velocities in the laboratory frame of reference $v_{ph}=2\pi f d/\alpha_{12}(f)$. The phase velocity of the modes at $r=+4$ cm measured from Fig. 7 is 1.5×10^3 m/s. For comparison the average velocity of a coherent dipole structure (a $m=1$ mode) measured at radius r is $2\pi f_p r$, where f_p is the peak frequency of the power spectrum. For $f_p\approx4$ kHz and $r=+4$ cm we find this velocity to be 1.0×10^3 m/s. Complete correspondence between these estimates should only be expected for a spectrum of linear wave modes (a sharply defined dispersion relation).

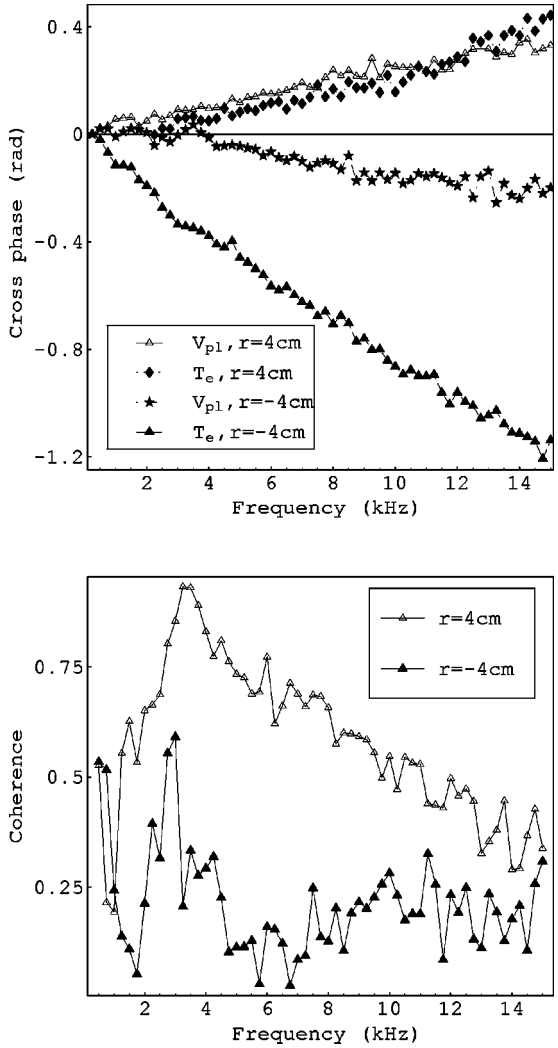

FIG. 7. Top: Cross-phase spectra between V_{pl} and T_e signals on two probes separated poloidally by 6 mm measured at $r=+4$ cm (two upper curves) and $r=-4$ cm (two lower curves). Bottom: Cross coherence between V_{pl} and T_e measured at $r=+4$ cm (upper curve) and $r=-4$ cm (lower curve).

The dispersion curves for $r=-4$ cm shows slowly propagating (0.5×10^3 m/s) flute modes governing the plasma potential fluctuations and fast (2.5×10^3 m/s) drift waves. The flute mode velocity in this position corresponds roughly to the $\mathbf{E}\times\mathbf{B}$ fluid flow velocity estimated from the measured potential profile. According to local, linear theory for flute modes in an unsheared flow [17], the phase velocity in the plasma frame of reference is of order 10 m/s, so this seems to be a reasonable result. The three times higher phase velocity (in the laboratory frame) measured at $r=+4$ cm, however, seems to be considerably higher than the poloidal rotation velocity of the fluid at any radial position. The discrepancy between observation and this simple theory should not come as a surprise, since the modes are not local, probably not linear, and the flow is strongly sheared.

The electron density and temperature profiles have a sharp gradient just inside the density peak. The electron diamagnetic velocity in this region is consistent with the high phase

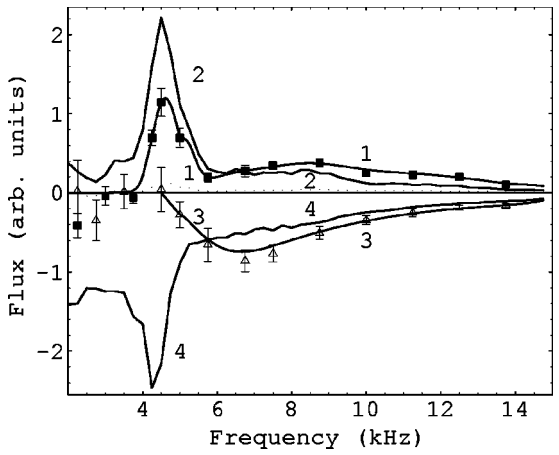

FIG. 8. Statistically averaged spectra of particle flux (1) and energy flux (2) as determined by Eqs. (1) and (2) at position $r=+6$ cm. Particle flux (3) and energy flux (4) at $r=-6$ cm.

velocity found for the plasma potential dispersion branch at $r=-4$ cm in Fig. 7, i.e., confirming our assumption that the plasma potential fluctuations are dominated by drift waves at this location.

The interpretation that two branches observed at $r=-4$ cm correspond to two different wave modes, while at $r=+4$ cm they correspond to the same mode, is confirmed by measurements of the cross coherence between plasma potential and electron temperature fluctuations in the two positions. The coherence spectra are presented in Fig. 7, and show very high coherence in the outside position (the two signals are created by the same mode) and very low coherence in the inside position (the two signals correspond to different modes, which are essentially uncorrelated).

Yet another evidence in support of the interpretation given above is obtained by the cross phase and cross coherence between V_{pl} and E. If only one mode branch influences V_{pl}, we would have that $E(f)=-ik(f)V_{pl}(f)$, the cross phase should be $3\pi/2$, and the coherence should be close to unity. If there are two mode branches, we have $V_{pl}=a_1\exp(ik_1y)+a_2\exp(ik_2y)$. In the $r=-4$ cm position, k_1 corresponds to drift waves and k_2 to flute modes, and we found that $k_2\approx 6k_1$. Evidence presented above indicates that the plasma potential fluctuations are dominated by drift waves, i.e., $a_1 \gg a_2$ and $V_{pl}\approx a_1\exp(ik_1y)$. However, the electric field becomes $E=-ik_1a_1\exp(ik_1y)-ik_2a_2\exp(ik_2y)$, and if $k_1a_1\sim k_2a_2$, we find that the cross phase between V_{pl} and E_y may differ strongly from $3\pi/2$, and since the electric field can have a substantial contribution from the flute-mode branch, the cross coherence may be substantially reduced. This is exactly what is observed in the inside position, while on the outside we find a cross phase of $3\pi/2$ and higher coherence.

D. Flux measurements

Particle fluxes calculated according to Eq. (1) for the probe positions $r=+6$ cm (curve 1) and $r=-6$ cm (curve 3) are presented in Fig. 8. Fluxes are statistically averaged with 0.25 kHz frequency resolution. For frequencies in the range 1.5–3 kHz the flux is zero within the statistical errors of measurements. It should also be noted that the coherence between n and E for frequencies in this interval is below 0.2, suggesting that the statistics should be improved for reliable flux measurements at these frequencies. For higher frequencies the length of the time series is sufficient for reliable measurements as is observed from decreasing error bars. For frequencies below 1.5 kHz the fluctuations are dominated by global oscillations involving the external circuit of the discharge. In this range the measurements of $\Gamma_x(f)$ are not reproducible. The reason for this is not yet completely understood.

From Fig. 8 one can see that the particle flux is directed down the gradient towards the wall on the outside as well as the inside slopes. At $r=+6$ cm roughly half of the particle flux is due to the large-scale coherent structures responsible for the spectral peak at $f=4.5$ kHz, and the rest is due to the turbulent spectrum on higher frequencies. At $r=-6$ cm most of the flux is due to the high frequencies. For both positions the cross phase α_{nE} is unfavorable for particle transport ($\alpha=\pi/2$ yields vanishing flux), so the deviation of α_{nE} from $\pi/2$ must be measured accurately in order to be able to obtain the flux density with a reasonable accuracy.

Energy fluxes calculated from Eq. (2) at $r=+6$ cm (curve 2) and $r=-6$ cm (curve 4) are also presented in Fig. 8. In both positions the flux is directed down the gradient and a major fraction of the flux is associated with the large-scale structures ($f<5$ kHz). Almost all of the energy flux is due to the second term in Eq. (2), i.e., it depends on the coherence and cross phase between $\tilde{T}_e$ and $\tilde{E}$. This cross-phase α_{TE} is close to $\pi/2$ on the outside and to π on the inside. This means that α_{TE} is unfavorable for energy transport on the outside. On the inside this cross phase is favorable for energy transport, which makes the energy flux here somewhat larger, even though the total power in the temperature fluctuations is considerably lower than on the outside slope.

The flux measurements show that the large-scale flute-mode structures play a substantial role in both particle and energy transport on the outside. On the inside only drift waves contribute to particle transport, while the coupling between temperature fluctuations in flute modes and electric field fluctuations in drift waves yields the major contribution to the energy transport.

The time-averaged radial particle flux densities measured at $r=\pm 6$ cm are $\langle\Gamma_r\rangle\approx 5\times 10^{18}$ m^{-2}s^{-1}. If one assumes that this value also corresponds to the spatially averaged radial flux density on a toroidal surface with minor radius 6 cm, we should have a total particle flux $\Phi=4\pi^2R_0r\langle\Gamma\rangle\approx 7.5\times 10^{18}$ s^{-1}. This should be compared to the total ionization rate due to the injected primary electrons. The upper limit of this ionization rate given by the injected power is $(I_{dis}/e)(\mathcal{E}_e/\mathcal{E}_i)=3.3\times 10^{19}$ s^{-1}. Here $\mathcal{E}_e=130$ V is the energy of the injected electrons and $\mathcal{E}_i\approx 24.6$ eV is the ionization energy for helium. If only a fraction of the energy of the primary electrons is available for ionization (i.e., if most of it ends up as radiated energy from excited atoms), the measured particle flux is consistent with this estimate. The plasma confinement time can be defined as $\tau_p=N_e/\Phi$, where $N_e=2\pi^2R_0r^2n_e=0.045n_e\approx 1.5\times 10^{16}$ m^{-1} is the

number of electrons inside the torus of minor radius 6 cm. With the measured particle flux this yields $\tau_p \approx 2$ ms.

The time-averaged radial energy flux density is measured to be $\langle Q_r \rangle \approx 2$ Wm^{-2} and the corresponding total energy flux is 3 W. The total injected power with $I_{dis}=1$ A is 140 W, implying that only about 2% of this power is transported to the wall as plasma energy. The remainder is radiated as emitted light from excited helium, consumed for ionization and for heating of neutrals via ion-neutral collisions.

V. DISCUSSION AND CONCLUSIONS

Measurements with the probe cluster applied here allow us to conclude that flute modes dominate all the fluctuations on the outer slope, while drift waves seem to dominate density and potential fluctuations on the inner slope, where flute modes are stable. Weak flute modes coexist with the drift waves on the inside slope, manifested through weak temperature fluctuations. The flute-mode spectrum exhibits a peak that is due to large-scale poloidally rotating structures, probably associated with the lowest poloidal wave number $(m=1)$. This is the fastest growing mode according to linear theory for flute interchange instability, but if the gradient is at the threshold for this instability, it also is the only linearly unstable mode. The higher wave numbers (corresponding to the power-law spectrum at higher frequencies) are driven unstable nonlinearly trough a turbulent cascade.

The purpose of this paper is to describe and demonstrate the power of a specific probe method, which applies to cold, weakly ionized, magnetized plasma. The method was applied to a particular plasma state, which was selected because it allowed us to make some comparisons to some results from linear stability theory for electrostatic flute modes and drift waves, and because it allowed identification of modes belonging to different dispersion branches. One should not get the impression, however, that the results obtained are universal for discharges in the simple torus. This type of a device is very versatile, and even with the present experimental setup there are a number of externally set parameters that determine the plasma state. The most important are the discharge current regulated by the heater current through the filament cathode, the discharge voltage determining the energy of the primary electrons and thereby the ionization rate, the neutral gas composition and pressure, and the magnetic field strength, which all influence the Pedersen conductivity σ_P and hence the depth and shape of the potential well. It is possible to obtain states with a deep concentric potential well with closed mean-flow surfaces encircling the plasma source region. For these states the radial transport must be anomalous, i.e., caused by fluctuations.

Other states are more influenced by the charge accumulation (vertical polarization) due to the curvature and gradient drifts, giving rise to a dipolelike potential structure. The convection pattern corresponding to this structure consists of a stationary double vortex, where the flow in the equatorial plane is directed outwards along the major radius, and hence the plasma produced in the center of the plasma column is transported to the wall by steady-state convection. These states are usually associated with very weak fluctuations.

For plasmas produced without electron injection, such as electron cyclotron resonance ionization [21], inductive discharges, or helicon discharges [22], the potential structure can be a positive hump. In these dicharges the situation can be quite similar to the potential well case in the sense that it has a poloidal rotation, flute modes may be unstable, and there may be large-scale coherent structures moving with the rotating plasma.

In hot cathode discharges the state studied in this paper can also be modified by changing the location of the cathode filament. By moving the filament a few centimeters to the inside the fluctuation characteristics are drastically changed. The fluctuation amplitudes increase by a factor of 3 and the cross phase between the density and plasma potential is different from that reported here. These changes may be related to the observation that the electron pressure profile is flatter, in particular, on the inside, and so is the potential gradient near the wall. The high fluctuation amplitudes and the cross phases observed suggest that the modes are no longer close to marginal stability, but so far these states are quite poorly understood.

The time series for $\tilde{n}$, $\tilde{V}_{pl}$, $\tilde{T}_e$, $\tilde{E}$, $\tilde{\Gamma}_x$, and $\tilde{Q}_x$ are stationary random signals, which can be made subject to statistical analysis. For instance, the probability distribution functions (PDFs) of $\Gamma_x(t)$ are non-Gaussian with fat tails. If $\tilde{n}$ and $\tilde{E}$ are Gaussian, it is easily shown that Γ_x has exponential tails [4]. On the inside of the torus, the tails are in fact exponential $[P(\Gamma_x) \sim \exp(-c|\Gamma_x|)]$, while on the outside they are algebraic $[P(\Gamma_x) \sim |\Gamma_x|^{-\xi}]$ with the power index $\xi \approx 2.7$. The PDF on the outside is consistent with a Lévy stable distribution, which physically implies an overrepresentation of large flux events (Lévy flights).

Results of the measurements for other plasma states, including more advanced statistical analysis and numerical simulations, will be published in forthcoming papers.

ACKNOWLEDGMENTS

The authors are grateful to G. Hellblom for his technical assistance, and O. E. Garcia, J. Juul Rasmussen, and V. Naulin for useful comments and discussions.

[1] D.W. Ross, Comments Plasma Phys. Controlled Fusion **12**, 155 (1989).
[2] P. Mantica, G. Vayakis, J. Hugill, S. Cirant, R.A. Pitts, and G.F. Matthews, Nucl. Fusion **31**, 1649 (1991).
[3] M. Endler *et al.*, Nucl. Fusion **35**, 1307 (1995).
[4] B.A. Carreras *et al.*, Phys. Plasmas **3**, 2664 (1996).
[5] J. Hugill, Plasma Phys. Controlled Fusion **42**, R75 (2000).
[6] H. Ji, H. Toyama, K. Miyamoto, S. Shinohara, and A. Fujisawa, Phys. Rev. Lett. **67**, 62 (1991).
[7] H.Y.W. Tsui *et al.*, Rev. Sci. Instrum. **63**, 4608 (1992).

[8] A.H. Nielsen, H.L. Pécseli, and J.J. Rasmussen, Phys. Plasmas **3**, 1530 (1996).
[9] S.V. Ratynskaia, V.I. Demidov, and K. Rypdal, Rev. Sci. Instrum. **71**, 1367 (2000).
[10] V.A. Roghanskii and L.D. Tsendin, Sov. Phys. Tech. Phys. **23**, 932 (1978).
[11] V.I. Demidov, S.V. Ratynskaia, R.J. Armstrong, and K. Rypdal, Phys. Plasmas **6**, 350 (1999).
[12] M.Y. Ye and S. Takamura, Phys. Plasmas **7**, 3457 (2000).
[13] E.J. Powers, Nucl. Fusion **14**, 794 (1974).
[14] K. Rypdal, E. Grøvoll, F. Øynes, Å. Fredriksen, R. Armstrong, J. Trulson, and H. L.Pēcseli, Plasma Phys. Controlled Fusion **36**, 1099 (1994).
[15] S.V. Ratynskaia, V.I. Demidov, and K. Rypdal, Rev. Sci. Instrum. **71**, 3382 (2000).
[16] K. Rypdal, H. Fredriksen, J.V. Paulsen, and O.M. Olsen, Phys. Scr., T **63**, 167 (1996).
[17] O.E. Garcia, J. Plasma Phys. **65**, 81 (2001).
[18] P. Satyanarayana, P.N. Guzdar, J.H. Huba, and S.L. Ossakow, J. Geophys. Lett. **89**, 2945 (1984).
[19] F. Øynes, H.L. Pecseli, and K. Rypdal, Phys. Rev. Lett. **75**, 81 (1995).
[20] F.J. Øynes, O.-M. Olsen, H.L. Pecseli, Å. Fredriksen, and K. Rypdal, Phys. Rev. E **57**, 2242 (1998).
[21] K. Rypdal, A.A. Fredriksen, O.M. Olsen, and G. Hellblom, Phys. Plasmas **4**, 1468 (1997).
[22] O. Grulke, F. Greiner, T. Klinger, and A. Piel, Plasma Phys. Controlled Fusion **43**, 525 (2001).